ISSN: 2579-5821 (Print)
ISSN: 2579-5546 (Online)
URL address: http://journal.unhas.ac.id/index.php/geocelebes
DOI: 10.70561/geocelebes.v10i1.43582

Jurnal Geocelebes Vol. 10 No. 1, April 2026, 48 – 68

Comparative Accuracy of Satellite-Derived Bathymetry Using Random Forest, Multiple Linear Regression, and Van Hengel and Spitzer Algorithm

Fathurrahman Apriliansyah[1], Muhammad Ulin Nuha[1]*, Aulia Try Atmojo[1], Kuncoro Teguh Setiawan[2], Aswar Syafnur[3]

[1]Geomatics Engineering, Faculty of Infrastructure and Regional Technology, Institut Teknologi Sumatera, Lampung 35365, Indonesia.
[2]Research Center for Geoinformatics, National Research and Innovation Agency, Cibinong 16911, Indonesia.
[3]Geophysics Department, Faculty of Mathematics and Natural Sciences, Hasanuddin University, Makassar 90245, Indonesia.

*Corresponding author. Email: muhammad.nuha@gt.itera.ac.id

Manuscript received: 23 March 2025; Received in revised form: 11 March 2026; Accepted: 26 March 2026

Abstract

Bathymetry mapping using conventional methods faces limitations in shallow waters. With the development of remote sensing technology, satellite-derived bathymetry (SDB) emerges as an alternative by utilizing wavelengths that penetrate water and capture depth information. This study compares the performance of three empirical SDB methods: Random Forest (RF), Multiple Linear Regression (MLR), and the Van Hengel and Spitzer (VHS) algorithm. SPOT 6 ORTHO-level satellite imagery and depth data from single beam echosounder measurements were used to construct the depth models. Model accuracy was evaluated using root mean square error (RMSE), mean absolute error (MAE), and total vertical uncertainty (TVU). Results show that the RF method achieves the highest accuracy across most depth ranges (1–5 m, 5–10 m, and 10–15 m), while the VHS algorithm performs best at 0–1 m. At depths beyond 15 meters, MLR shows relatively better performance compared to other methods, although overall uncertainty remains high. Based on the coefficient of determination (R^2), RF achieves the best result with a value of 0.610, followed by MLR with 0.462, and VHS with 0.313. These findings highlight the superior adaptability of the RF method in estimating bathymetry across varying depth zones using optical satellite imagery.

Keywords: Multiple Linear Regression; Random Forest; Satellite-Derived Bathymetry; Van Hengel and Spitzer Algorithm

Citation: Apriliansyah, F., Nuha, M. U., Atmojo, A. T., Setiawan, K. T., & Syafnur, A. (2026). Comparing Accuracy of Satellite-Derived Bathymetry Using Random Forest, Multiple Linear Regression, and Van Hengel and Spitzer Algoritm. *Jurnal Geocelebes*, 10(1): 48–68, doi: 10.70561/geocelebes.v10i1.43582

Introduction

Bathymetry measurement or sea depth mapping has a very crucial role in various fields, such as maritime navigation, marine resource management, and marine environmental studies. Bathymetry or sea depth is a measure of the depth of marine waters measured from the water surface to the seabed. The need for bathymetry estimation information is also driven by activities in the area around the coast such as development activities, port activities, fishing, dredging, oil mining, and aquaculture (Pushparaj & Hegde, 2017).

Bathymetry mapping continues to progress. In general, bathymetry mapping is carried out by conventional methods, which is the echosounder method. But this method has shortcomings, which is the limitations of bathymetry measurements in shallow waters which are very difficult to do because of difficulties in navigation so that the ship does not sink and the presence of coral reefs in shallow waters can cause data to be inaccurate.

Bathymetry data acquisition is increasingly experiencing development with the advent of technology. One of the methods often used to obtain bathymetry information by utilizing technology is Satellite Derived Bathymetry (SDB). Remote sensing technology in obtaining point information depth information in shallow water by utilizing wavelengths that has a good spectral response to water and can penetrate certain depths depending on the capabilities of each satellite sensor (Nugraha et al., 2017).

The basic principle behind optical satellite-derived bathymetry is that different wavelengths exhibit different attenuation rates in water, which control depth sensitivity and effective penetration range (Wei et al., 2021; IHO, 2024). The different penetration behaviors of optical wavelengths in the water column are illustrated in Figure 1.

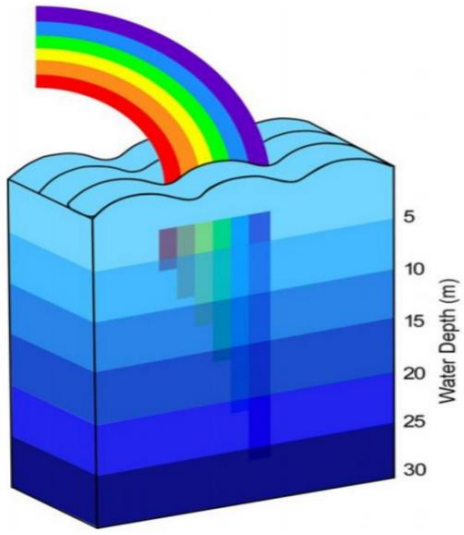

Figure 1. Wavelength penetration in water (Purkis, 2019).

Based on Figure 1 presented, the shorter the electromagnetic wavelength, the deeper the penetration of the wave. This is consistent with wavelength-dependent attenuation behavior reported in recent empirical assessments (Wei et al., 2021; IHO, 2024). The depth of penetration also depends on the level of water turbidity.

Optical penetration is limited by water turbidity and light attenuation (Kd). In clear waters, blue–green wavelengths may reach 15–20 m, but in most coastal waters, reliable SDB rarely exceeds 20–25 m (Gao, 2009; Manessa et al., 2016; Cahalane et al., 2019). Beyond this depth, bottom reflectance becomes undetectable, and depth estimates rely more on statistical extrapolation than true optical signal. Accordingly, depth estimates exceeding 20–25 m derived from optical satellite imagery should not be interpreted as true bathymetric measurements, but rather as statistical extrapolations beyond the effective optical penetration range. In the absence of detectable bottom reflectance, such estimates do not represent physically meaningful seabed depth and must be treated with caution or excluded from accuracy assessment (Caballero & Stumpf, 2020a; Cahalane et al., 2019). Recent best-practice guidance recommends that SDB products explicitly report their effective depth range and uncertainty, and that areas lacking a detectable bottom signal should be masked or excluded to avoid misleading depth interpretation (IHO, 2024).

Water quality is a critical control on the reliability of optical SDB because increasing turbidity and chlorophyll concentration reduce bottom detectability and therefore limit depth retrieval accuracy. Caballero & Stumpf (2019) emphasized that evaluating turbidity effects is essential both for selecting suitable satellite scenes and for understanding the practical limitations of SDB in optically complex waters.

Satellite-Derived Bathymetry has two methods: empirical method and analytical method. Analytical modeling of bathymetry is based on the way light propagates in water. The formation of this model requires the input of several optical properties of water, such as water coefficient, attenuation coefficient and backscattering (Gao, 2009). In empirical

modeling, the relationship between the remotely sensed radiance of a water body and the depth at the sample location is established empirically without regard to how light is transmitted in water (Gao, 2009). In this study, three methods are used to predict depth, which are the random forest (RF) method, multiple linear regression (MLR) and, the Van Hengel and Spitzer (VHS) algorithm.

Although empirical satellite-derived bathymetry models do not explicitly solve the radiative transfer equation, they implicitly approximate the physical interaction between water depth, bottom reflectance, and wavelength-dependent light attenuation in the water column. Shorter wavelengths, particularly in the blue and green spectral regions, exhibit lower attenuation coefficients and higher depth sensitivity, while longer wavelengths are rapidly absorbed. As a result, empirical models statistically approximate these optical processes without requiring direct measurements of inherent optical properties, making them suitable for shallow-water applications when bottom reflectance remains detectable (Gao, 2009; Pahlevan et al., 2017; Caballero & Stumpf, 2020a).

Recent developments in satellite-derived bathymetry have increasingly focused on the application of machine learning techniques to overcome the limitations of traditional empirical models. Recent research also shows that RF can be used not only to estimate water depth but also to automatically identify valid and invalid bathymetric pixels in satellite-derived bathymetry products, thereby improving the reliability of SDB mapping in complex coastal environments (Sharr et al., 2024). Studies employing RF, Gaussian Process Regression, and other multivariate learning approaches have demonstrated improved accuracy in capturing non-linear depth–reflectance relationships, particularly in optically complex and heterogeneous coastal waters (Ashphaq et al., 2024; Sagawa et al., 2019). Recent studies have also incorporated attention mechanisms into machine learning models to better capture spatial dependencies in multispectral imagery, leading to improved bathymetric inversion performance in optically complex coastal waters (Fang et al., 2024). Compared to earlier Indonesian case studies, this research extends previous work by systematically evaluating classical empirical models and machine learning approaches using SPOT-6 imagery, while explicitly addressing depth-dependent performance and uncertainty characteristics. Recent studies further demonstrate that RF-based SDB models benefit from the use of multi-date satellite imagery and careful image quality control, as bathymetric accuracy is strongly influenced by the quality and suitability of the input reflectance data (Mudiyanselage et al., 2022). Multi-temporal Sentinel-2 imagery has also been used to derive shallow-water bathymetry with RMSE values typically between 1.4 and 2.6 m when compared with LiDAR reference data (Evagorou et al., 2019). In addition to multispectral imagery, several recent studies have explored the integration of satellite optical data with spaceborne LiDAR measurements such as ICESat-2 to improve training data availability and enhance bathymetric prediction accuracy (Xie et al., 2023). Machine learning models combining ICESat 2 photon counting LiDAR bathymetric points with Sentinel 2 reflectance data have demonstrated high inversion accuracies for shallow water bathymetry in coastal regions, highlighting the value of hybrid active–passive data fusion approaches in SDB (Ye et al., 2024). Time-series or clean-coastal-water composite satellite imagery has been shown to improve the stability of satellite-derived bathymetry compared with single-date images, particularly when combined with RF regression and evaluated against hydrographic accuracy standards (Munawaroh et al., 2024). Recent studies

also explore iterative fusion methods that leverage active lidar photon returns and passive optical pseudo photons to enhance satellite derived bathymetry accuracy in both clear and turbid coastal waters (Hu et al., 2025).

Recent studies have shown that RF-based SDB can improve model generalization when trained using multi-temporal optical imagery rather than a single scene. The use of repeated Sentinel-2 observations also provides a practical means to improve SDB in environments with variable turbidity. Caballero and Stumpf (2020b) showed that multi-image approaches can support more routine and spatially scalable bathymetry mapping by exploiting the high revisit frequency of Sentinel-2A/B, particularly in data-poor or remote coastal regions. Sagawa et al. (2019) developed a generalized shallow-water bathymetry model using RF and 135 Landsat-8 images, reporting an RMSE of 1.41 m for depths between 0 and 20 m, which demonstrates the potential of multi-temporal machine learning approaches for improving SDB robustness across different sites.

In Indonesia, linear regression methods such as MLR are still widely used for bathymetry modeling because they are simple and easy to implement (Manessa et al., 2016). Machine learning approaches such as RF are also proven to provide high accuracy in capturing the non-linear relationship between reflectance and depth (Dewi et al., 2021). In addition, VHS spectral transformation methods have also been applied in several local studies (Nisa et al., 2023). Manessa et al. (2016) applied RF for SDB in Indonesian waters using WorldView-2 imagery. However, their study did not compare RF with MLR and the VHS algorithm using SPOT-6 imagery. Therefore, this study contributes by evaluating these three empirical methods specifically for Bawean Island using SPOT-6 data.

The principle of a RF is to create a random sample of training data with the same distribution across all trees in the forest. The MLR method forms a model that correlates the dependent and independent variables. The last method used in this research is the method with the VHS algorithm. This algorithm is a development of an algorithm previously known by Lyzenga. The principle of this algorithm is to transform the value of satellite images to obtain the relative depth of seawater using a rotational transformation matrix.

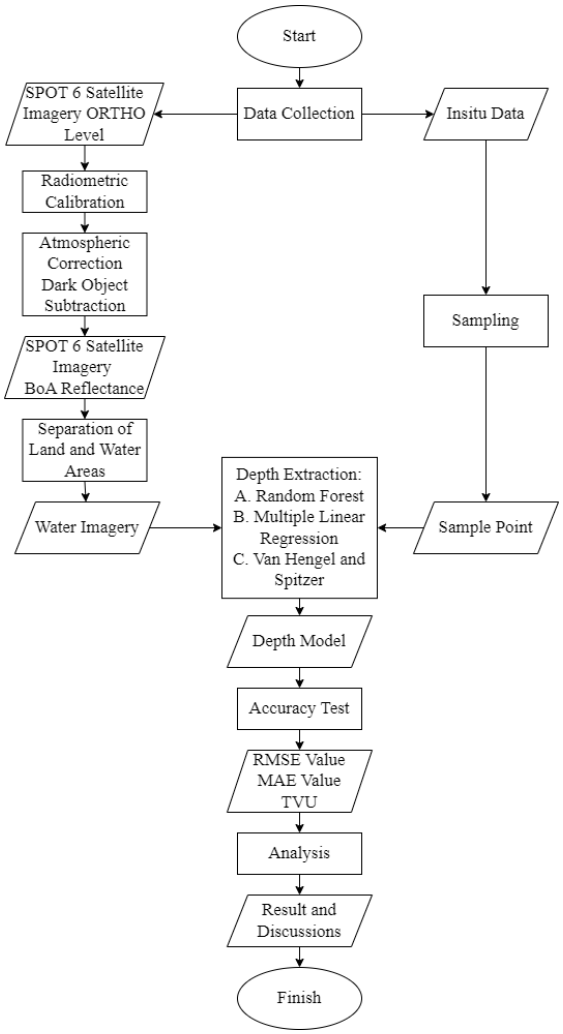

Figure 2. Flowchart.

The image used in this study is the SPOT 6 ORTHO level satellite image with a resolution of 6 meters. The image was subjected to radiometric calibration and atmospheric correction to obtain surface reflectance values. This research aims to analyze the accuracy produced by the three

methods in their ability to extract shallow water bathymetry. The overall workflow of the research process is presented in Figure 2.

Materials and Methods

The research site was located in the waters of Bawean Island, Gresik Regency, East Java. The geographical location of the study area is shown in Figure 3. The location was chosen based on the availability of data from the National Research and Innovation Agency (BRIN).

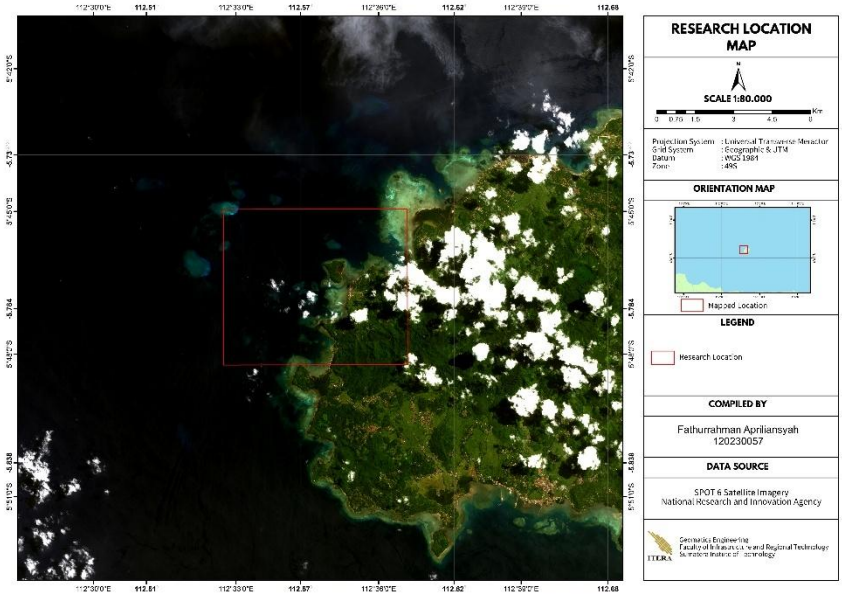

Figure 3. Research location.

Image Pre-processing

The image preprocessing stage aims to prepare the image data before further analysis. Radiometric correction is required to improve the visual quality of the image and adjust the pixel values to match the original spectral reflectance or radiance of an object. The main source of error is caused by atmospheric disturbances because it uses energy from electromagnetic radiation. Atmospheric effects alter the spectral signal recorded by satellite sensors, causing deviations between the measured reflectance and the true surface reflectance of objects. In this study, radiometric calibration and atmospheric correction processes were carried out.

To convert image data in digital number format into radians and/ or reflectance values requires a radiometric calibration stage. The radians value can also be converted to the Top of Atmosphere (ToA) reflectance value. To convert image pixel values to reflectance values, use Equation 1 (Nisa et al., 2023).

$$\rho_\lambda = \frac{\pi L_\lambda d^2}{ESUN_\lambda sin\theta} \quad (1)$$

Description:
L_λ : radians ($Wm^{-2}Sr^{-1}$)
D : earth-sun distance
$ESUN_\lambda$: solar irradiance ($Wm^{-2}\mu m$)
θ : solar elevation (°)

After the radiometric calibration process, the atmospheric correction process is then carried out. This research uses the Dark Object Subtraction (DOS) method of atmospheric correction. The DOS method converts satellite reflectance values into surface reflectance values. In the absence of atmospheric layers, dark objects such as

water and cloud shadows should have a pixel value of zero, if an object has a non-zero pixel value then the value is considered as bias (Nisa et al., 2023). The DOS method takes several samples of deep-sea pixels in each channel, and then the minimum value of the sample is used as a subtraction factor for the pixel value in each channel. The result of atmospheric correction is an image with a reflectance value below the atmosphere (Bottom of Atmosphere (BoA)). The DOS atmospheric correction calculation uses Equation 2 (Nisa et al., 2023).

$$L'_i = L_i - L_{si} \quad (2)$$

Description:
L'_i : corrected pixel value on band i
L_i : initial pixel value of band i
L_{si} : minimum pixel value of band i

Furthermore, the image masking process is used to separate land and water areas. In this research, the masking process is carried out using the Normalized Difference Vegetation Index (NDVI) method with the addition of Decision Tree rules. Satellite imagery preprocessing, including water masking and spectral filtering, is an important step in satellite-derived bathymetry workflows to ensure that depth inversion models are applied only to valid water pixels. The calculation of the NDVI method uses Equation 3 (Chybicki et al., 2023).

$$\text{NDVI} = \frac{\text{Red}-\text{NIR}}{\text{Red}+\text{NIR}} \quad (3)$$

Description:
Red : Digital Number in the red band
NIR : Digital Number in the NIR band

The Decision Tree rule is used to remove cloudy areas in the image by utilizing the NDVI value, where values less than -0.1 are considered as water.

Random Forest (RF)

RF is one of the machine learning algorithms that can be used for satellite-based bathymetry depth extraction. RF is a clustering algorithm that uses the bootstrap aggregating method by utilizing a number of decision trees to generate predictions (Bramante et al., 2013). The term “random forest” is derived from two words, the first being the word random, which refers to the random sampling of data from the original data set, and the second being forest, which refers to the construction of many decision trees from randomly sampled data (Mabula et al., 2023).

The RF model is operated by making random samples from the training data with the same distribution on all trees in the forest (Dewi et al., 2021). Mabula et al. (2023) mentioned that the RF model will automatically form a decision tree using the training data. The training data includes measured water depth and spectral values from satellite images as predictor variables (Syaiful et al., 2019). The final prediction result of RF is the average of all the results of the decision tree and will be influenced by the correlation between the trees.

Multiple Linear Regression (MLR)

Linear regression forms a model that correlates the dependent and independent variables. A linear regression will be called a simple linear regression if it only has one independent variable, while if it has more than one independent variable, it is called multiple linear regression (Dewi et al., 2021). The correlation between the dependent and independent variables is modeled by a linear function and its parameters are estimated from the data.

In this study, a MLR model was built using reflectance values from the red, green and blue channels that had been transformed using the natural logarithm. This transformation follows Lyzenga (1978), who demonstrated that the reflectance–depth relationship is exponential and must be linearized using logarithmic transformation before regression. This transformation was done because the relationship between water surface

reflectance and water depth is exponentially decreasing. Therefore, the conventional linear regression approach will only produce a less representative model if no transformation is performed. Lyzenga (1978) stated that the logarithmic transformation is used to transform the exponential relationship into a linear relationship that can be modeled statistically. The application of log transformation to reflectance is also used in various SDB studies, including by Manessa et al. (2016) who used a similar approach on WorldView-2 images in shallow waters of Indonesia.

This logarithmic transformation approach has been consistently adopted in recent empirical SDB studies to address the exponential attenuation of light in the water column. Studies have demonstrated that applying linear regression directly to raw reflectance values results in biased depth estimates, whereas log-transformed reflectance improves model stability, reduces systematic error, and preserves physical interpretability of the regression coefficients (Caballero & Stumpf, 2020a; Dewi & Rizaldy, 2021).

The MLR method performs image analysis by using multiple linear regression methods between field depth (in-situ) and multispectral images, then used to obtain regression coefficients (Nisa et al., 2023). The equation used to extract depth using the MLR method is written in Equation 4 (Manessa et al., 2016; Nisa et al., 2023).

$$Z = M_0 + M_{blue} \cdot \ln(B_{blue}) + M_{green} \cdot \ln(B_{green}) + M_{red} \cdot \ln(B_{red}) \quad (4)$$

Description:
Z : absolute depth
M_0 : constant
M_{blue} : blue channel coefficient
M_{green} : green channel coefficient
M_{red} : red channel coefficient
B_{blue} : blue channel reflectance spectral value
B_{green} : green channel reflectance spectral value
B_{red} : red channel reflectance spectral value

Van Hengel and Spitzer Algorithm (VHS)

The VHS algorithm is a development of the algorithm previously introduced by Lyzenga. The algorithm formulated by Van Hengel & Spitzer (1991) is an algorithm that transforms the value of satellite images to obtain the relative depth of seawater. The transformation process is done using a rotation transformation matrix. Van Hengel & Spitzer (1991) mentioned that water depth is directly proportional to the radiance/radiation algorithm and the relative water depth value can be obtained by performing a special transformation on the radiance value of each band. The VHS Equation 5–8 is formulated as follows (Van Hengel & Spitzer, 1991).

$$Ur = \frac{VarGreen + VarBlue}{2 * CoVarGreenBlue} \quad (5)$$

$$Us = \frac{VarRed + VarBlue}{2 * CoVarRedBlue} \quad (6)$$

$$R = \text{Arctan}(U_r + \sqrt{(Ur^2) + 1} \quad (7)$$

$$S = \text{Arctan}(U_s + \sqrt{(Us^2) + 1} \quad (8)$$

Description:
R : angle of rotation direction (Green-Blue channel)
S : angle of rotation direction (Red-Blue channel)
VarGreen : variation of 30 green channel data
VarBlue : variation of 30 blue channel data
VarRed : variation of 30 red channel data
CoVarGrenBlue : covariance of green and blue channels
CoVarRedBlue : covariance of red and blue channels

The results of the S and R angle calculation operations are then used to calculate the depth index value. The equation for

calculating the depth index is found in Equation 9 (Van Hengel & Spitzer, 1991).

$$X = (\mathrm{Cos}(R) * \mathrm{Sin}(S) * B1) + (\mathrm{Sin}(R) * \mathrm{Cos}(S) * B2) + (\mathrm{Sin}(S) * B3) \quad (9)$$

Description:
X : relative depth
B1 : reflectance value of the blue channel
B2 : reflectance value of the green channel
B3 : reflectance value of the red channel

Accuracy Test

In hydrographic contexts, vertical accuracy and uncertainty are commonly evaluated within standardized survey frameworks, such as those described in the IHO S-44 standard and satellite-derived bathymetry best-practice guidance (IHO, 2020). The field data used is the in situ depth. Based on the Regulation of the Head of the Geospatial Information Agency (Perka BIG) Number 18 of 2020 concerning Procedures for the Implementation of Geospatial Information, there are four general approaches used to conduct validation. Common approaches to test the accuracy of depth extraction results are Root mean square error (RMSE), coefficient of determination (R^2), Mean average error (MAE), and Total Vertical Uncertainty (TVU).

RMSE is the root of the average number of squares of the difference between the in situ depth value and the depth value from BBS processing using the depth algorithm (Nisa et al., 2023). The result of RMSE is the error rate of the depth extraction model. Lower RMSE values indicate higher model accuracy because they represent smaller differences between predicted and observed depths. A smaller RMSE value means that the depth extraction model is better than a larger RMSE value. The equation for evaluating the accuracy test using RMSE is as follows in Equation 10 (BIG, 2021).

$$\mathrm{RMSE}_{(\mathrm{depth})} = \sum \sqrt{\frac{(Y_i - Y'_i)^2}{N}} \quad (10)$$

Description:
Y_i : In-situ depth
Y'_i : Depth of satellite-derived bathymetry results
n : Number of depth samples used

RMSE and MAE are two standard metrics widely used in model evaluation, and reporting both is common practice because they emphasize different characteristics of model error distributions (Hodson, 2022). MAE can be operated using Equation 11 (BIG, 2021).

$$\mathrm{MAE} = \frac{1}{n}\sum_{i=1}^{n}|x_i - \hat{x}_i| \quad (11)$$

Description:
x_i : Depth of satellite-derived bathymetry results
$\hat{x}_i$: In-situ depth
n : Number of depth samples used

The coefficient of determination is between zero and one. If the R^2 value approaches one, the influence of the independent variable on the dependent variable is stronger. The equation for calculating the coefficient of determination is Equation 12 (BIG, 2021).

$$R^2 = 1 - \frac{\text{explained variance}}{\text{total variance}} \quad (12)$$

The last test performed is the calculation of Total Vertical Uncertainty (TVU). IHO standardization has an accuracy test method known as TVU. Referring to the hydrographic survey manual S-44 edition issued by IHO (2020), TVU is a component of total propagated uncertainty (TPU) calculated in vertical dimensions. TVU is a one-dimensional quantity with all vertical measurement uncertainties included. TVU can be operated using Equation 13 (BIG, 2021).

$$\mathrm{TVU}_{\max}(d) = \pm\sqrt{a^2 + (b \times d)^2} \quad (13)$$

Description:
a : Depth-independent error factor
b : Depth-dependent error factor
d : SDB model depth value
b x d : Depth-dependent uncertainty parameter

Table 1. Maximum value of TVU for 95% confidence level (IHO, 2020)

Orde	a (m)	b
Exclusive	0.15	0.0075
Special	0.25	0.0075
1a/1b	0.50	0.0130
2	1.00	0.0230

The coefficients a and b can be seen in the IHO SP-44 document in Table 1.

Results and Discussion

Radiometric and Atmospheric Correction

The images obtained are still images with pixel values in the form of digital numbers (DN). The DN value must be converted into a reflectance value so that it can be used to obtain relative depth. The value obtained from the Equation 1 is the ToA reflectance value presented in Figure 4.

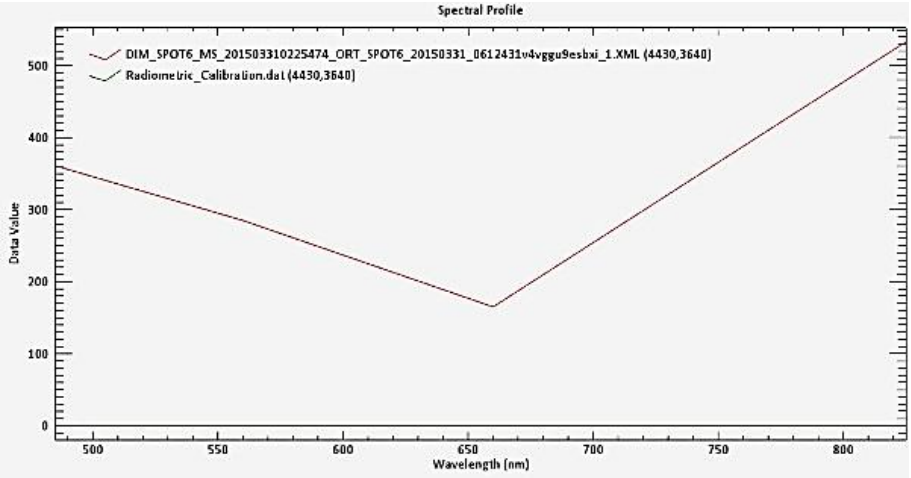

Figure 2. Pixel value of atmospheric correction image.

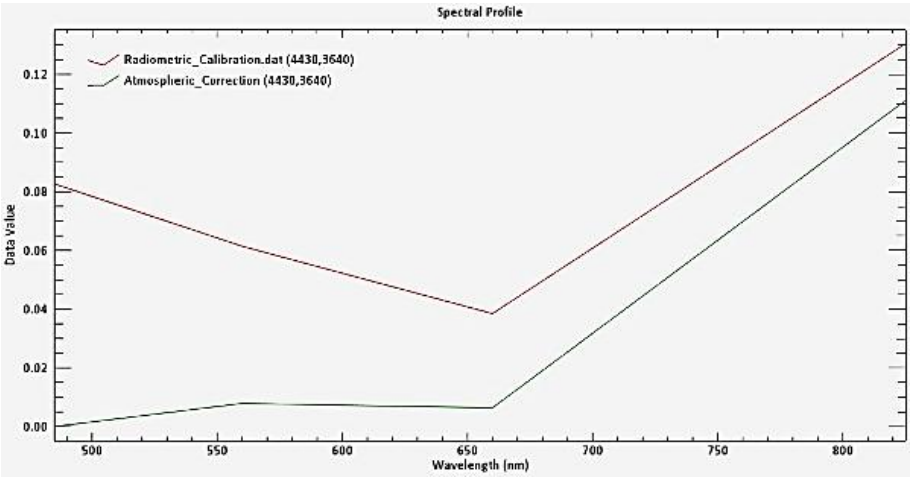

Figure 3. Pixel value of radiometric calibration image

Image pixel values that have been radiometrically calibrated range from zero to one. The pixel value of the image that has been radiometrically calibrated is the ToA reflectance value that does not represent the value of the object's reflection on the earth's surface. This is because in the process of recording from satellite imagery, there is scattering of electromagnetic waves caused by the presence of gas and dust particles in the atmosphere. A comparison of the reflectance values in the image before atmospheric correction and the image after atmospheric correction is presented in Figure 5.

Correction with the DOS method can be done because in deep water areas electromagnetic wave energy is absorbed, so the reflectance that appears from the

inside can be assumed to be atmospheric reflectance. Images that have been corrected for atmospheric effects can be used for bathymetry extraction. The corrected image is presented in Figure 6.

Image Masking

The use of water areas is necessary so that the process of extracting depth values using satellite imagery only involves spectral values present in the water. In the NDVI index value generated at the research location, cloudy areas are identified with a value range of -0.2 to -0.1. Based on this range of values, cloudy areas can be removed by providing rules on the decision tree with NDVI values less than -0.1 designated as waters. The NDVI classification results with the decision tree rule are presented in Figure 7.

Figure 4. Visual corrected image.

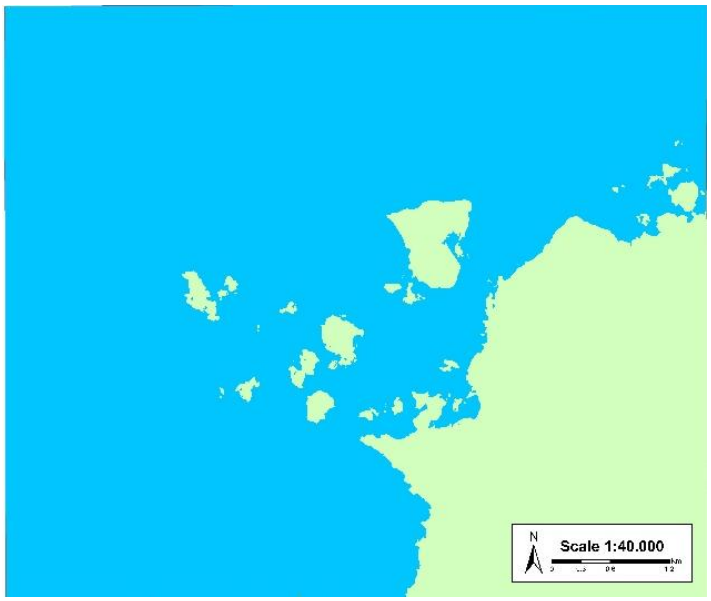

Figure 5. NDVI reclassification result.

The results of NDVI reclassification which are still in raster format become input data that will be converted into vector format. The raster data were converted into vector format through a standard conversion process in GIS software, so that the

classified water areas could be separated more clearly. The vector format classification results then removed the land part and left the water part. The data will be used for image masking in each band. The visual appearance of the extracted water area after masking is shown in Figure 8. Restricting satellite-derived bathymetry predictions to optically shallow water is essential, because accuracy decreases rapidly beyond depths where bottom reflectance is detectable; therefore, masking unsuitable pixels is required to ensure that mapped bathymetry remains fit for purpose (Richardson et al., 2025).

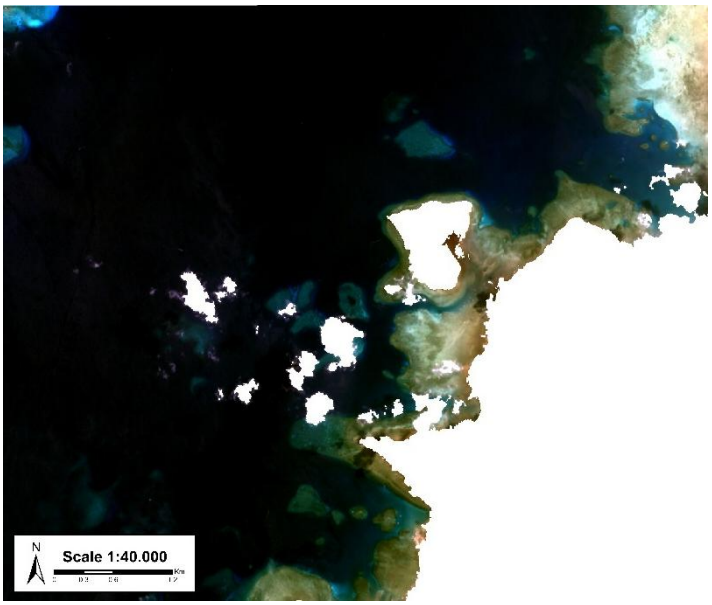

Figure 6. Visual water imagery.

Depth Extraction Results

The depth value obtained from each method produces different depths. The composite band used is the RGB band composite of the SPOT 6 satellite image. Although the RF model produced depth values up to 36.1 m, depths beyond 20–25 m likely do not represent true optical bathymetry due to light attenuation limitations. This behavior is consistent with recent studies indicating that RF-based SDB models often outperform traditional empirical approaches, while their effective depth range typically remains within approximately 10–20 m depending on water clarity and seabed conditions (Kwon et al., 2024). The results of the RF method extraction are presented in Figure 9.

There are several parameters used in processing the RF method, one of which is the variation in the number of trees (ntree). Based on Safi'i & Dewi (2020), ntree variation does not have a significant effect on the results of the SDB model, so the ntree variation used is the default setting from SDB GUI, which is 300. The train dataset is also needed in RF processing, which is 10%. A 10% training dataset was selected to avoid overfitting while still providing sufficient samples for model learning, following common practice in previous SDB studies (Safi'i & Dewi, 2020; Ashphaq et al., 2024). The remaining 90% of data were used as an independent validation set. The accuracy test process refers to horizontal and vertical accuracy with a 90% confidence level. So the training data used is 10% and the data for accuracy testing is 90%. The depth extraction results obtained using the MLR method are shown in Figure 10.

The depth extraction results obtained with the MLR method produce varied values. But there is still a depth estimation error

shown in the black part. The depth estimate obtained in the area is less than 0 meters, which means the value is negative. The negative depth result is an error because the depth value should be positive. According to Syaiful et al. (2019), depth values below 0 must be eliminated because it is a depth values with a high error rate.

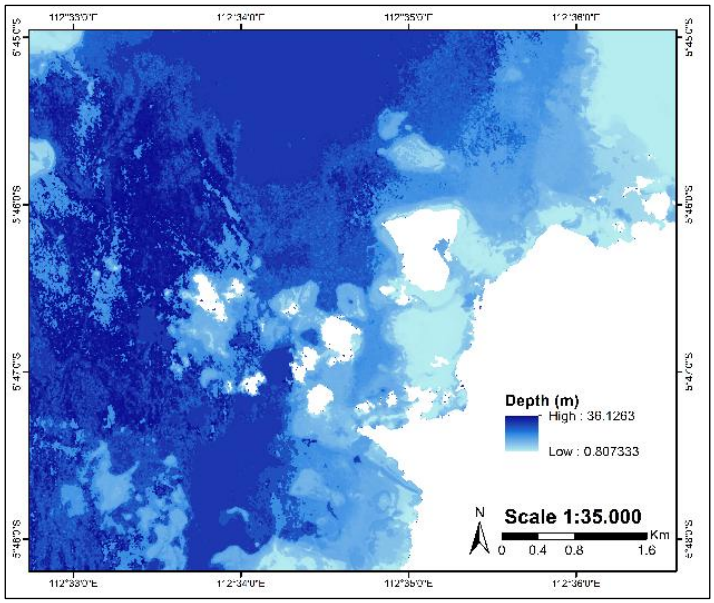

Figure 7. Results of depth extraction of RF method.

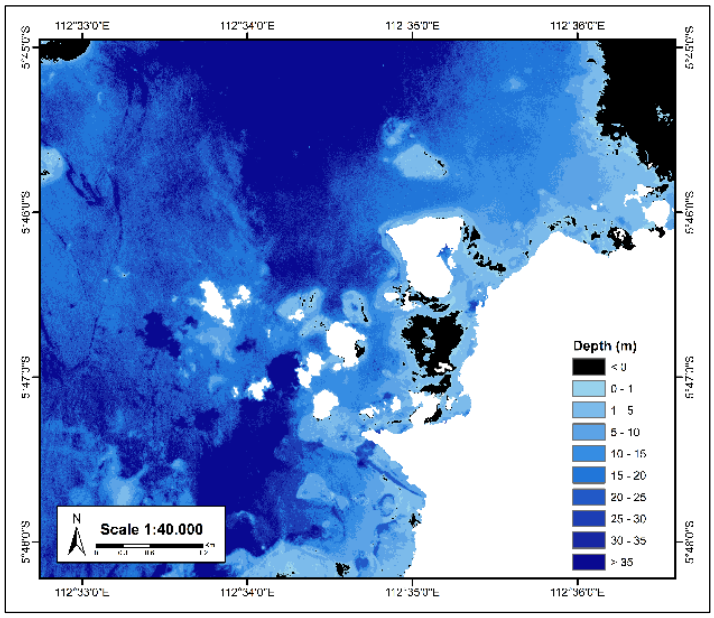

Figure 8. Depth extraction results of MLR method.

Negative depth estimates were excluded from subsequent accuracy assessment, as they are physically unrealistic and indicate model extrapolation beyond valid spectral response ranges. Similar filtering procedures have been applied in previous satellite-derived bathymetry studies to maintain physical consistency and avoid bias in model evaluation (Dewi & Rizaldy, 2021; Caballero & Stumpf, 2020a). The absolute depth results derived from the VHS algorithm are presented in Figure 11.

The absolute depth of the VHS algorithm gets a depth range of less than 0 to more than 15 meters. The maximum depth obtained from this method is 20.1 meters. The maximum depth is smaller than the

other two methods used in this study. The depth obtained also still has estimation errors in areas with black color. This is indicated by the depth of the area which is negative. This error is the same as the error obtained with the multiple linear regression method. Negative depth estimates were excluded from further analysis as they are physically unrealistic.

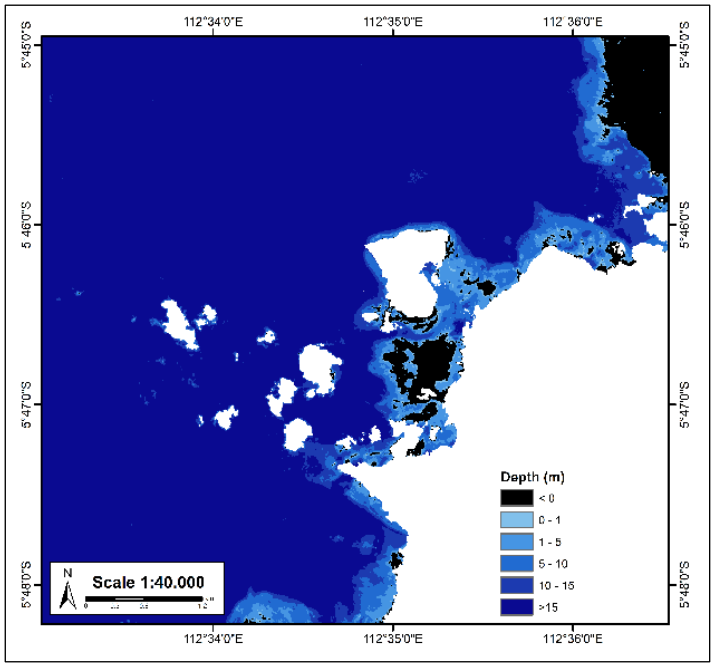

Figure 9. Absolute depth results of VHS algorithms.

Accuracy Test

The level of accuracy in the estimation model can be seen from the resulting RMSE and MAE values. The smaller the value, the higher the accuracy of the model. This study uses comparison data sourced from direct observations in the field using a single beam echosounder. The calculation of RMSE and MAE values is done per depth.

In addition to numerical accuracy metrics, scatterplots of predicted versus in-situ depths were generated for each model to visually evaluate model performance, bias, and error dispersion. Scatterplot analysis is essential to identify systematic overestimation or underestimation patterns and the presence of outliers that may not be fully captured by RMSE, MAE, or R^2 values alone (Ashphaq et al., 2024; Sagawa et al., 2019).

Based on the resulting RMSE values in Table 2 and MAE values in Table 3, the VHS algorithm produces the lowest error at a depth of 0–1 meter, with RMSE of 0.518 meters and MAE of 0.424 meters. At depths of 1–5 meters, 5–10 meters, and 10–15 meters, the RF method consistently yields the lowest errors, with RMSE values of 3.045, 6.827, and 12.491 meters respectively, and MAE values of 2.816, 6.715, and 12.417 meters. At depths exceeding 15 meters, the MLR method shows slightly better performance with RMSE of 18.120 meters and MAE of 17.900 meters. These results indicate that the RF method is the most accurate overall within the typical SDB depth range, while VHS is more suitable for very shallow areas, and MLR performs relatively better in deeper waters. Similar comparative studies in highly dynamic coastal environments report that machine learning approaches tend to reduce systematic bias relative to traditional empirical models,

although careful masking and validation remain essential to avoid overconfident extrapolation (Quang et al., 2025).

Table 2. Comparison of RMSE values.

Method	Depth (m)				
	0-1	1-5	5-10	10-15	>15
Random Forest	0.545	3.045	6.827	12.491	18.121
Multiple Linear Regression	0.613	3.221	7.703	12.325	18.120
Van Hengel and Spitzer	0.518	3.300	7.493	12.328	17.967

Table 3. Comparison of MAE values

Method	Depth (m)				
	0-1	1-5	5-10	10-15	>15
Random Forest	0.463	2.816	6.715	12.417	18.013
Multiple Linear Regression	0.545	3.009	7.576	12.244	17.900
Van Hengel and Spitzer	0.424	3.079	7.397	12.262	17.846

Table 4. Comparison of coefficient of determination

Method	R^2
Random Forest	0.687
Multiple Linear Regression	0.436
Van Hengel and Spitzer	0.444

Figure 12 presents the scatterplot of in-situ versus predicted depths for the RF model. Figure 13 presents the scatterplot of in-situ versus predicted depths for the MLR model. Figure 14 presents the scatterplot of in-situ versus predicted depths for the VHS algorithm.

Based on Table 4 presented, the highest coefficient of determination is generated by the RF method which is 0.687. Then continued by the VHS algorithm with an R^2 value of 0.444. The last is the MLR method with an R^2 value of 0.436. This indicates that the RF method has a strong correlation with insitu depth data. In contrast, the method that has the weakest correlation is produced by the MLR method.

Based on BIG Regulation No. 18 of 2021, testing of the SDB model is also carried out by calculating the total vertical uncertainty (TVU). TVU describes the total uncertainty in water depth measurement.

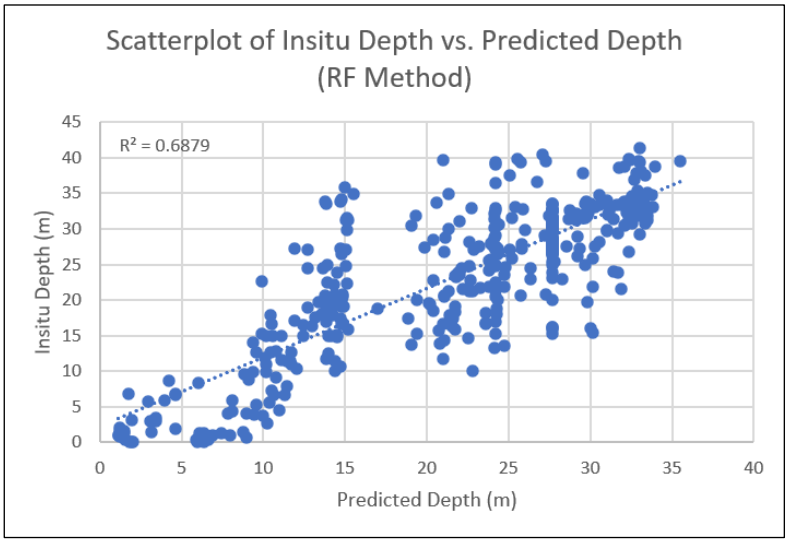

Figure 10. Scatterplot of in-situ and predicted depth (RF).

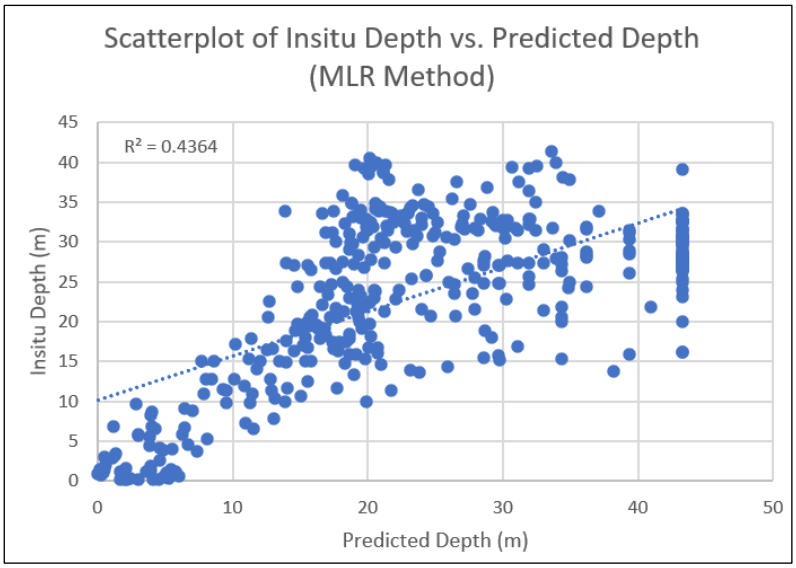

Figure 11. Scatterplot of in-situ and predicted depth (MLR).

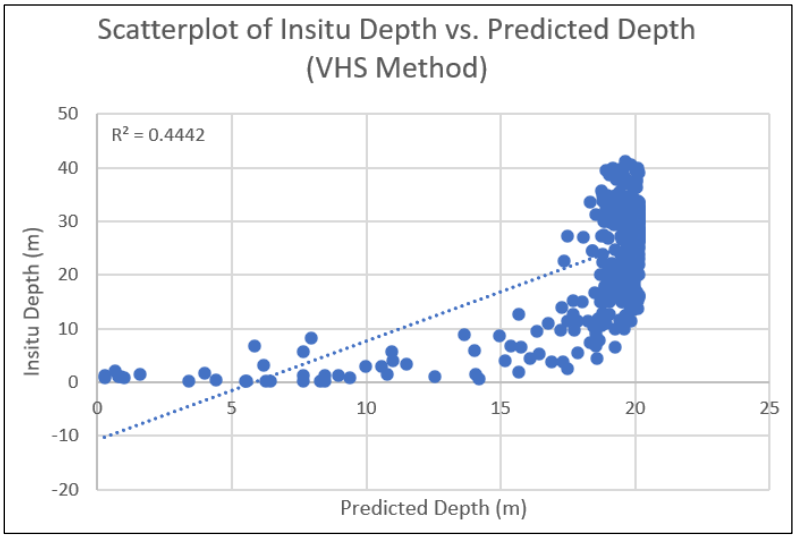

Figure 12. Scatterplot of in-situ and predicted depth (VHS).

Table 5. Random Forest method TVU testing.

Depth (m)	Inbound Data (%)				Data not entered (%)
	2	1a/1b	Special	Exclusive	
0-5	4.17	16.67	8.33	16.67	54.17
5-10	3.70	7.41	0.00	0.00	88.89
10-15	8.11	4.05	1.35	1.35	85.14
15-20	11.76	0.00	0.00	0.00	88.24
20-25	9.20	3.45	0.00	0.00	83.91
>25	12.23	6.38	2.13	2.13	71.28

Table 6. Multiple Linear Regression method TVU testing.

Depth (m)	Inbound Data (%)				Data not entered (%)
	2	1a/1b	Special	Exclusive	
0-5	18.92	5.41	0.00	0.00	75.68
5-10	0.00	13.64	0.00	0.00	86.36
10-15	3.13	3.13	0.00	3.13	90.63
15-20	6.82	3.41	0.00	2.27	87.50
20-25	1.41	1.41	0.00	1.41	95.77
>25	4.19	0.60	1.20	0.60	93.41

Table 7. Van Hengel and Spitzer method TVU testing.

Depth (m)	Inbound Data (%)				Data not entered (%)
	2	1a/1b	Special	Exclusive	
0-5	20.00	0.00	20.00	20.00	40.00
5-10	6.25	6.25	0.00	0.00	87.50
10-15	0.00	0.00	0.00	0.00	100.0
15-20	4.00	0.80	2.40	1.60	91.20
>20	0.00	0.77	0.00	1.54	97.69

Based on the TVU testing of the three SDB methods, it shows a similar trend with vertical uncertainty increasing with depth. The VHS algorithms tend to have a higher percentage of data not in any order at deeper depths, indicating a significant level of uncertainty. The RF method performed slightly better at shallower depths, with a greater percentage of data falling into the TVU order. The MLR method showed variation in its results, with some depth ranges having lower uncertainties than others, but still showing high uncertainties at deeper depths. This comparison indicates that despite variations in the accuracy of each method, vertical uncertainty remains a major challenge in depth measurement using the SDB technique, especially at deeper depths.

The TVU test results above show that the VHS algorithms perform best at shallow depths (0–5 meters) with 60% of the data falling into the TVU order, which is the highest percentage compared to other methods at the same depth range. Although vertical uncertainty remains a challenge at deeper depths, these algorithms generally show the highest level of accuracy at shallow depths compared to the RF and MLR methods. However, for deeper depths, none of the methods consistently showed a significant advantage. Each method has a high degree of uncertainty, so the selection of the best method may also depend on the depth range favored in a particular research or application.

There are several factors that can affect the accuracy of the SDB model. The bathymetry data generated from satellite image estimation has a weakness in its limited ability to penetrate waves in the water column. Penetration of light through the water column, the intensity will decrease exponentially with increasing depth (attenuation) (Prasetya et al., 2023). Organic and inorganic particles can reduce the intensity of light penetrating the water column. Cahalane et al. (2019) also said that in general the SDB model is strongly influenced by the type of sensor, water quality and other environmental conditions.

Recent studies also highlight that the accuracy of SDB is influenced not only by environmental conditions but also by how spectral input data and reference measurements are prepared prior to modeling. Lee et al. (2025) demonstrated that the configuration of spectral inputs and the spatial interpolation strategy used for reference depth data can significantly affect model performance. Their results indicate that different combinations of spectral bands, preprocessing strategies, and interpolation approaches may lead to substantial variations in predicted bathymetric accuracy, emphasizing the importance of carefully designing the input data structure when developing SDB models.

The main limitation in optical image-based bathymetry methods is the ability of light to penetrate the water column. Physics based satellite derived bathymetry methods applied to multispectral imagery, such as Landsat OLI, integrate optical water properties and bottom reflectance to optimize bottom unmixing and can achieve RMSE values mostly less than 2 m even in waters as deep as 30 m, demonstrating physical modelling as a complementary

SDB strategy (Kim et al., 2024). According to Gao (2009), the blue to green wavelengths (0.48–0.60 µm) commonly used in satellite imagery can only penetrate depths of up to 15–20 meters in clear, calm waters. Even under optimum conditions, the detectable depth rarely exceeds 20 meters and the uncertainty can reach more than 4–5 meters. Gao also emphasized that if the waters have high turbidity, the maximum detectable depth will be much shallower. In this study, the bathymetry model does not explicitly include turbidity parameters or light diffusion coefficient (Kd), so depth predictions above 25 meters need to be considered carefully as they may fall outside the effective spectral penetration range of SPOT-6 imagery. Therefore, depth estimates beyond 25 m in this study should be interpreted with caution and are not recommended for operational hydrographic use.

Recent machine learning studies also indicate that SDB accuracy is not controlled only by depth itself, but also by water-quality-dependent optical properties and by the relevance of the predictor variables used in the model. Liu et al. (2024) found that models incorporating QAA-derived inherent optical properties can match or outperform models using reflectance alone, especially in turbid waters, and they further showed that including excessive redundant bands may reduce model accuracy rather than improve it.

Conclusion

Based on the resulting RMSE and MAE values, at a depth of 0–1 meter, the VHS algorithms produce the lowest RMSE and MAE values, which are 0.518 meters and 0.424 meters. At a depth of 1–5 meters, the RF method produces the lowest values, which are RMSE of 3.045 meters and MAE of 2.816 meters. At a depth of 5–10 meters, the RF method produces the lowest value, which are RMSE of 6.827 meters and MAE of 6.715 meters. At a depth of 10–15 meters, the MLR method produces the lowest value, which are RMSE of 12.325 meters and MAE of 12.244 meters. At depths >15 meters, the VHS algorithms produce the lowest value, which are RMSE of 17.967 meters and MAE of 17.846 meters. Based on the R^2 value obtained, the RF method produces the best R^2 value of 0.687. Furthermore, the VHS algorithm with an R^2 value of 0.444 and the last is the MLR method with an R^2 value of 0.436.

Acknowledgements

The author would like to express his deepest gratitude to all those who have contributed to the making of this article so that this article can be completed.

Author Contribution

In compiling this research journal, each author is divided into several job desks. **Conceptualization**: Fathurrahman Apriliansyah, Muhammad Ulin Nuha, Aulia Try Atmojo; **Methodology**: Fathurrahman Apriliansyah, Muhammad Ulin Nuha, Aulia Try Atmojo, Kuncoro Teguh Setiawan; **Writing-Original Draft Preparation**: Fathurrahman Apriliansyah, Muhammad Ulin Nuha, Aswar Syafnur; **Writing-Review and Editing**: Fathurrahman Apriliansyah, Muhammad Ulin Nuha, Aulia Try Atmojo, Kuncoro Teguh Setiawan, Aswar Syafnur; **Visualization**: Fathurrahman Apriliansyah, Aulia Try Atmojo, Aswar Syanur. All authors have read and agreed to the published version of the manuscript.

Conflict of Interest

The author declares no financial or personal connections with any organization or parties involved in this research. Therefore, the research findings are solely the author's responsibility.

References

Ashphaq, M., Srivastava, P. K., & Mitra, D.

(2024). Satellite - Derived Bathymetry in Dynamic Coastal Geomorphological Environments Through Machine. *Earth and Space Science*, 11(7), 1–23. https://doi.org/10.1029/2024EA003554

BIG. (2021). *Peraturan Badan Informasi Geospasial Republik Indonesia Nomor 18 Tahun 2021 Tentang Tata Cara Penyelenggaraan Informasi Geospasial*. Badan Informasi Geospasial. https://peraturan.bpk.go.id/Details/217091/peraturan-big-no-18-tahun-2021

Bramante, J. F., Raju, D. K., & Sin, T. M. (2013). Multispectral derivation of bathymetry in Singapore's shallow, turbid waters. *International Journal of Remote Sensing*, 34(6), 2070–2088. https://doi.org/10.1080/01431161.2012.734934

Caballero, I., & Stumpf, R. P. (2019). Preliminary Assessment of Turbidity and Chlorophyll Impact on Bathymetry Derived from Sentinel-2A and Sentinel-3A Satellites in South Florida. *Remote Sensing*, 11(6), 645. https://doi.org/10.3390/rs11060645

Caballero, I., & Stumpf, R. P. (2020a). Atmospheric correction for satellite-derived bathymetry in the Caribbean waters : from a single image to multi-temporal approaches using Sentinel-2A/B. *Optics Express*, 28(8), 11742–11766. https://doi.org/10.1364/OE.390316

Caballero, I., & Stumpf, R. P. (2020b). Towards Routine Mapping of Shallow Bathymetry in Environments with Variable Turbidity : Contribution of Sentinel-2A/B Satellites Mission. Remote Sensing, 12(3), 451. https://doi.org/10.3390/rs12030451

Cahalane, C., Magee, A., Monteys, X., Casal, G., Hanafin, J., & Harris, P. (2019). A comparison of Landsat 8, RapidEye and Pleiades products for improving empirical predictions of satellite-derived bathymetry. *Remote Sensing of Environment*, 233, 111414. https://doi.org/10.1016/j.rse.2019.111414

Chybicki, A., Sosnowski, P., Kulawiak, M., Bieliński, T., Korlub, W., Łubniewski, Z., Kempa, M., & Parzuchowski, J. (2023). Study of various machine learning approaches for Sentinel-2 derived bathymetry. *PLoS ONE*, 18(9), e0291595. https://doi.org/10.1371/journal.pone.0291595

Dewi, R. S., & Rizaldy, A. (2021). Accuracy Assessment of Satellite Derived Bathymetry Model for Depth Extraction in Sorong Shallow Water Area Accuracy Assessment of Satellite Derived Bathymetry Model for Depth Extraction in Sorong Shallow Water Area. *IOP Conference Series: Earth and Environmental Science*, 925, 012053. https://doi.org/10.1088/1755-1315/925/1/012053

Dewi, R. S., Rizaldy, A., Hartanto, P., & Suprajaka, S. (2021). Assesing The Accuracy of Shallow Water Depth Estimation by Using Multispectral Satellite Images. *Geographia Technica*, 16(Special Issue), 180–197. http://dx.doi.org/10.21163/GT_2021.163.14

Evagorou, E., Mettas, C., Agapiou, A., Themistocleous, K., & Hadjimitsis, D. (2019). Bathymetric maps from multi-temporal analysis of Sentinel-2 data: the case study of Limassol, Cyprus. *Advances in Geosciences*, 45, 397–407, https://doi.org/10.5194/adgeo-45-397-2019

Fang, S., Wu, Z., Wu, S., Chen, Z., Shen, W., & Mao, Z. (2024). Enhancing Water depth inversion accuracy in turbid coastal environments using random forest and coordinate attention mechanisms. *Frontiers in Marine Science*, 11, 1471695. https://doi.org/10.3389/fmars.2024.1471695

Gao, J. (2009). Bathymetric mapping by

means of remote sensing: Methods, accuracy and limitations. *Progress in Physical Geography*, 33(1), 103–116. https://doi.org/10.1177/0309133309105657

Hodson, T. O. (2022). Root-mean-square error (RMSE) or mean absolute error (MAE): when to use them or not. *Geoscientific Model Development*, 15, 5481–5487. https://doi.org/10.5194/gmd-15-5481-2022

Hu, Q., Li, J., & Cheng, L. (2025). Satellite-derived bathymetry based on iterative fusion of active lidar photons and passive pseudo- photons. *International Journal of Digital Earth*, 18(1), 2543568. https://doi.org/10.1080/17538947.2025.2543568

IHO. (2020). *International Hydrographic Organization Standards for Hydrographic Surveys*. *377*.

IHO. (2024). *International Hydrographic Organization Guidance to Satellite-Derived Bathymetry © Copyright International Hydrographic Organization 2024. 377*.

Kim, M., Danielson, J., Storlazzi, C., & Park, S. (2024). Physics-Based Satellite-Derived Bathymetry (SDB) Using Landsat OLI Images. *Remote Sensing*, 16(5), 843. https://doi.org/10.3390/rs16050843

Kwon, J-Y., Shin, H-K., Kim, D-H., Lee, H-G., Bouk, J-K., Kim, J-H., & Kim, T-H. (2024). Estimation of shallow bathymetry using Sentinel-2 satellite data and random forest machine learning : a case study for Cheonsuman, Hallim, and Samcheok Coastal Seas. *Journal of Applied Remote Sensing*, 18(1), 014522. https://doi.org/10.1117/1.JRS.18.014522

Lee, S-J., Kim, H-S., Yun, H-S., & Lee, S-H. (2025). Satellite-Derived Bathymetry Using Sentinel-2 and Airborne Hyperspectral Data : A Deep Learning Approach with Adaptive Interpolation. *Remote Sensing*, 17(15), 2594. https://doi.org/10.3390/rs17152594

Liu, Z., Liu, H., Ma, Y., Ma, X., Yang, J., Jiang, Y., & Li, S. (2024). Exploring the Most Effective Information for Satellite-Derived Bathymetry Models in Different Water Qualities. *Remote Sensing*, 16(13), 2371. https://doi.org/10.3390/rs16132371

Lyzenga, D. R. (1978). Passive remote sensing techniques for mapping water depth and bottom features. *Applied Optics*, 17(3), 379–383. https://doi.org/10.1364/ao.17.000379

Mabula, M. J., Kisanga, D., & Pamba, S. (2023). Application of machine learning algorithms and Sentinel-2 satellite for improved bathymetry retrieval in Lake Victoria, Tanzania. *Egyptian Journal of Remote Sensing and Space Science*, 26(3), 619–627. https://doi.org/10.1016/j.ejrs.2023.07.003

Manessa, M. D. M., Kanno, A., Sekine, M., Haidar, M., Yamamoto, K., Imai, T., & Higuchi, T. (2016). Satellite-Derived Bathymetry Using Random Forest Algorithm and Worldview-2 Imagery. *Geoplanning: Journal of Geomatics and Planning,* 3(2), 117–126. https://doi.org/10.14710/geoplanning.3.2.117-126

Mudiyanselage, S. S. J. D., Wilkinson, B., & Lecours, V. (2022). Satellite-derived bathymetry using machine learning and optimal Sentinel-2 imagery in South- West Florida coastal waters. *GIScience & Remote Sensing*, 59(1), 1143–1158. https://doi.org/10.1080/15481603.2022.2100597

Munawaroh, M., Wicaksono, P., Farda, N. M., Lumban-Gaol, Y., Khakhim, N., & Kamal, M. (2024). Performance test of clean-coastal-water composite sentinel 2A image for shallow water bathymetry mapping. *Remote Sensing Applications: Society and*

Environment, 35, 101212. https://doi.org/10.1016/j.rsase.2024.101212

Nisa, S. Q., Karang, I. W. G. A., Putra, I. D. N. N., Setiawan, K. T., & Aziz, K. (2023). Perbandingan Akurasi Metode Empiris untuk Pemetaan Batimetri Perairan Benoa, Bali, Menggunakan Citra Satelit SPOT. *Journal of Marine Research and Technology*, 6(1), 60. https://doi.org/10.24843/jmrt.2023.v06.i01.p09

Nugraha, A. Y., Prayudha, B., Ibrahim, A. L., & Riyadi, N. (2017). Pemetaan Batimetri di Perairan Dangkal menggunakan Data Penginderaan Jauh Spot-7 (Studi Kasus Lembar-Lombok). *Jurnal Chart Datum*, 3(2), 61–80. https://doi.org/10.37875/chartdatum.v3i2.120

Pahlevan, N., Sarkar, S., Franz, B. A., Balasubramanian, S. V, & He, J. (2017). Remote Sensing of Environment Sentinel-2 MultiSpectral Instrument (MSI) data processing for aquatic science applications: Demonstrations and validations. *Remote Sensing of Environment*, 201, 47–56. https://doi.org/10.1016/j.rse.2017.08.033

Prasetya, M. I., Siregar, V. P., & Agus, S. B. (2023). Comparison of Satellite-Derived Bathymetry Algorithm Accuracy Using Sentinel-2 Multispectral Satellite Image. *Jurnal Kelautan Tropis*, 26(1), 113–125. https://doi.org/10.14710/jkt.v26i1.16050

Purkis, S. J. (2019). Remote Sensing Coral Reefs. In *Encyclopedia of Ocean Sciences, Third Edition: Volume 1-5* (3rd ed., Vols. 1–5). Elsevier Inc. https://doi.org/10.1016/B978-0-12-409548-9.10813-9

Pushparaj, J., & Hegde, A. V. (2017). Estimation of bathymetry along the coast of Mangaluru using Landsat-8 imagery. *Journal of Ocean and Climate: Science, Technology and Impacts*, 8(2), 71–83. https://doi.org/10.1177/1759313116679672

Quang, N. H., Banno, M., & Ha, N-T. (2025). Satellite derived bathymetry using empirical and machine learning approaches: a case study in the highly dynamic coastal water. *Coastal Engineering Journal*, 67(2), 232–251. https://doi.org/10.1080/21664250.2024.2445418

Richardson, G., Knudby, A., Wu, Y., & Ansari, M. (2025). A case study comparing approaches to mask satellite-derived bathymetry. *Discover Geoscience*, 3, 103. https://doi.org/10.1007/s44288-025-00219-1

Safi'i, A. N., & Dewi, R. S. (2020). Uji Akurasi Metode Berbasis Citra Satelit untuk Ekstraksi Data Batimetri. *Teknik*, 41(2), 142–151. https://doi.org/10.14710/teknik.v0i0.29516

Sagawa, T., Yamashita, Y., Okumura, T., & Yamanokuchi, T. (2019). Shallow Water Bathymetry Derived by Machine Learning and Multitemporal Satellite Images. *International Geoscience and Remote Sensing Symposium (IGARSS)*, 8222–8225. https://doi.org/10.1109/IGARSS.2019.8899043

Sharr, M. B., Parrish, C. E., & Jung, J. (2024). International Journal of Applied Earth Observation and Geoinformation Automated classification of valid and invalid satellite derived bathymetry with random forest. *International Journal of Applied Earth Observation and Geoinformation*, 129, 103796. https://doi.org/10.1016/j.jag.2024.103796

Syaiful, S. N., Helmi, M., Widada, S., Widiaratih, R., Subardjo, P., & Suryoputro, A. A. D. (2019). Analisis Digital Citra Satelit Worldview-2 untuk Ekstraksi Kedalaman Perairan

Laut di Sebagian Perairan Pulau Parang, Kepulauan Karimunjawa, Provinsi Jawa Tengah. *Indonesian Journal of Oceanography*, 1(1), 36–43. https://doi.org/10.14710/ijoce.v1i1.6262

Van Hengel, W., & Spitzer, D. (1991). Multi-temporal water depth mapping by means of landsat TM. *International Journal of Remote Sensing*, 12(4), 703–712. https://doi.org/10.1080/01431169108929687

Wei, C., Zhao, Q., Lu, Y., & Fu, D. (2021). Assessment of Empirical Algorithms for Shallow Water Bathymetry Using Multi-Spectral Imagery of Pearl River Delta Coast, China. *Remote Sensing*, 13(16), 3123. https://doi.org/10.3390/rs13163123

Xie, C., Chen, P., Zhang, Z., & Pan, D. (2023). Satellite-derived bathymetry combined with Sentinel-2 and ICESat-2 datasets using machine learning. *Frontiers in Earth Science*, 11, 1111817. https://doi.org/10.3389/feart.2023.1111817

Ye, M., Yang, C., Zhang, X., Li, S., Peng, X., Li, Y., & Chen, T. (2024). Shallow Water Bathymetry Inversion Based on Machine Learning Using ICESat-2 and Sentinel-2 Data. *Remote Sensing*, 16(23), 4603. https://doi.org/10.3390/rs16234603